

# SCIENTIFIC REPORTS



OPEN

## Identification and characterization of the structure–activity relationships involved in UGT1A1 inhibition by anthraquinone and dianthrone constituents of *Polygonum multiflorum*

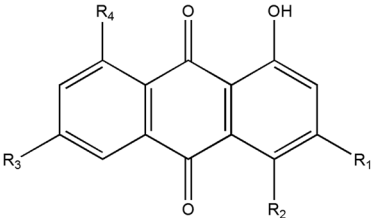
Qi Wang<sup>1,2</sup>, Yadan Wang<sup>2</sup>, Yong Li<sup>1</sup>, Binyu Wen<sup>3</sup>, Zhong Dai<sup>2</sup>, Shuangcheng Ma<sup>1,2</sup> & Yujie Zhang<sup>1</sup>

The adverse effects of *Polygonum (P.) multiflorum*, including abnormal bilirubin metabolism, are a serious public health issue. As uridine diphosphate (UDP)-glucuronosyltransferase 1A1 (UGT1A1) is the only enzyme responsible for bilirubin metabolism, we investigated the inhibitory effect of a *P. multiflorum* extract and 10 anthraquinone and dianthrone compounds on UGT1A1 in rat liver microsomes *in vitro*. The *P. multiflorum* extract exhibited the strongest inhibitory effect on UGT1A1 activity (inhibition constant [ $K_i$ ] = 0.3257  $\mu$ M, 1422  $\mu$ g of material/mL), followed by cis-emodin dianthrone ( $K_i$  = 0.8630  $\mu$ M), trans-emodin dianthrone ( $K_i$  = 1.083  $\mu$ M), emodin-8-O-gluc ( $K_i$  = 3.425  $\mu$ M), and polygonumnlolide C2 ( $K_i$  = 4.291  $\mu$ M). Analysis of the structure–activity relationships of these compounds suggested that the spatial orientation of the molecules and the presence of particular functional groups affect UGT1A1 inhibition. A mechanistic analysis showed that all the tested compounds docked into two of the nine active sites of UGT1A1 and suggested that hydrophobic interactions and hydrogen bonds are important for the affinity of the tested compounds for UGT1A1; moreover, their interaction energies were generally in agreement with the  $K_i$  values. These findings provide insight into adverse reactions to *P. multiflorum* and identify the pharmacophores involved in inhibition of UGT1A1.

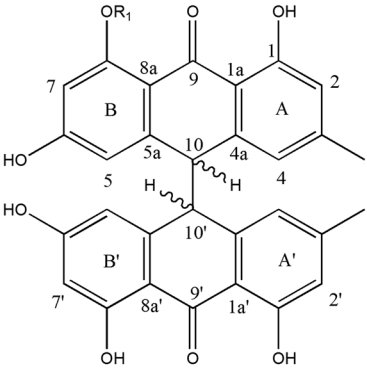
*P. multiflorum* (common names: *Polygonum multiflorum* Thunb<sup>1</sup>, Polygoni Multiflora Radix<sup>2</sup>, *Fallopia multiflora*, Heshouwu<sup>3</sup>, fleecflower root<sup>4,5</sup>, Polygoni multiflori<sup>6</sup>, and foti root<sup>7</sup>) is among the most frequently used medicinal plants in China. The main components of this plant are flavonoids<sup>1,8–11</sup>, quinones, and anthrones<sup>12</sup>, which are used as ingredients in various medicines. The major quinone constituents of *P. multiflorum* have multiple biological activities, exerting antimicrobial, antioxidant, and anti-human cytomegalovirus effects<sup>13</sup>. However, *P. multiflorum* reportedly also exerts adverse effects<sup>14–18</sup>, the most common and serious of which is abnormal bilirubin metabolism<sup>19–21</sup>. Also, anthraquinones can lead to elevated total bilirubin levels and induce hepatotoxicity<sup>22–30</sup>.

Uridine diphosphate (UDP)-glucuronosyltransferases (UGTs) are an important family of phase II drug-metabolizing enzymes that play major roles in the elimination and detoxification of endogenous and exogenous compounds<sup>31–33</sup>. UGT1A1 is the only UGT isoform involved in the metabolic clearance of bilirubin, which is a toxic waste product of heme degradation<sup>34</sup>. The inhibition of UGT1A1 may therefore lead to bilirubin accumulation, which can induce, for example, jaundice, liver dysfunction, and carcinogenesis<sup>35–38</sup>.

<sup>1</sup>Beijing University of Chinese Medicine, Beijing, 100029, China. <sup>2</sup>National Institutes for Food and Drug Control, Beijing, 100050, China. <sup>3</sup>Dongfang Hospital, Beijing University of Chinese Medicine, Beijing, 100078, China. Correspondence and requests for materials should be addressed to S.M. (email: [masc@nifdc.org.cn](mailto:masc@nifdc.org.cn)) or Y.Z. (email: [zhyj227@126.com](mailto:zhyj227@126.com))



Compound	R <sub>1</sub>	R <sub>2</sub>	R <sub>3</sub>	R <sub>4</sub>
emodin	H	H	OH	OH
physcion	H	H	OCH <sub>3</sub>	OH
rhein	COOH	H	H	OH
citreorosein	H	OH	OH	OH
Emodin-8-O-glc	H	H	OH	Glu

Compound	C <sub>10</sub>	C <sub>10'</sub>	R <sub>1</sub>
polygonumnolide C2	α H	α H	Glu
polygonumnolide C3	β H	α H	Glu
polygonumnolide C4	α H	β H	Glu
trans-emodin dianthrone	α H/β H	β H/α H	H
cis-emodin dianthrone	α H/β H	α H/β H	H

**Figure 1.** Chemical structures of 10 *P. multiflorum* compounds.

Therefore, we hypothesized that the abnormal bilirubin metabolism and hyperbilirubinemia observed following administration of *P. multiflorum* could be a result of UGT1A1 inhibition, primarily by quinones.

We tested this hypothesis previously by administering a 70% ethanol extract of *P. multiflorum* orally to rats, which resulted in marked inhibition of UGT1A1 activity<sup>39</sup>. Furthermore, we recently demonstrated that emodin competitively inhibits UGT1A1 in three model systems ( $K_i = 5.400 \pm 0.956$  ( $p < 0.05$ ) in the HLM system,  $10.02 \pm 0.611$  ( $p < 0.05$ ) in the RLM system, and  $4.850 \pm 0.528$  ( $p < 0.05$ ) in the rUGT1A1 system). The degree of inhibition of rat and human UGT1A1 did not differ significantly<sup>40</sup>.

In the present study, we used a sensitive and robust *in vitro* assay to investigate UGT1A1 inhibition by a *P. multiflorum* extract and 10 individual components in a rat liver microsomes (RLM) system<sup>41</sup>. The monomer components tested were emodin-type anthraquinones and dianthrone derivatives (Fig. 1). Based on the results, we discuss the relationships between the structures of these compounds and their inhibitory effects on UGT1A1. Moreover, a mechanistic analysis was performed by the molecular docking method. Our findings will facilitate further studies of the mechanisms underlying the toxicity of *P. multiflorum*.

## Results

**Inhibitory effects of *P. multiflorum* extract and its constituents on UGT1A1.** Different concentrations of an ethanol *P. multiflorum* extract and its 10 major components were screened for their inhibition of

No.	Drugs	Mode of inhibition	$K_i$ value ( $\mu\text{M}$ )
a	Polygonum multiflorum extracts	Competitive inhibition	0.3257
b	Emodin	Competitive inhibition	10.01
c	Physcion	Non-Competitive inhibition	94.75
d	Rhein	Mixed Type inhibition	127.3
e	Citreorosein	Mixed Type inhibition	18.56
f	Emodin-8-O-glc	Competitive inhibition	3.425
g	Polygonumolide C2	Non-Competitive inhibition	4.291
h	Polygonumolide C3	Non-Competitive inhibition	12.89
i	Polygonumolide C4	Un-Competitive inhibition	77.42
j	Trans-emodin dianthrone	Competitive inhibition	1.083
k	Cis-emodin dianthrone	Competitive inhibition	0.8630

**Table 1.** Modes of inhibition and  $K_i$  values for inhibition of UGT1A1-mediated metabolism by *P. multiflorum* extracts and 11 of its components in rat liver microsomes.

UGT1A1 activity in RLM. The second plots of the slopes of the Lineweaver–Burk plots were used to calculate  $K_i$  values. The modes of inhibition were competitive, non-competitive, mixed-competitive, and un-competitive (Table 1 and Supplementary Fig. S1). *P. multiflorum* extract ( $K_i = 0.3257 \mu\text{M}$ , 1422  $\mu\text{g}$  of material/mL) exhibited the strongest inhibition of UGT1A1. The rank order of UGT1A1 inhibitory potency of the 10 tested major compounds was cis-emodin dianthrone ( $K_i = 0.8630 \mu\text{M}$ ) > trans-emodin dianthrone ( $K_i = 1.083 \mu\text{M}$ ) > emodin-8-O-glc ( $K_i = 3.425 \mu\text{M}$ ) > polygonumolide C2 ( $K_i = 4.291 \mu\text{M}$ ) > emodin ( $K_i = 10.01 \mu\text{M}$ ) > polygonumolide C3 ( $K_i = 12.89 \mu\text{M}$ ) > citreorosein ( $K_i = 18.56 \mu\text{M}$ ) > polygonumolide C4 ( $K_i = 77.42 \mu\text{M}$ ) > physcion ( $K_i = 94.75 \mu\text{M}$ ) > rhein ( $K_i = 127.3 \mu\text{M}$ ).

**Structure–activity relationships.** The structure–activity relationships of the tested compounds were evaluated. Emodin, physcion, rhein, citreorosein, and emodin-8-O-glu have the same skeleton type with different substituents (Fig. 1). Among them, emodin exhibited moderate inhibitory activity against UGT1A1 ( $K_i = 10.01 \mu\text{M}$ ). Introduction of a hydroxyl group at the 4-position resulted in slightly decreased activity ( $K_i = 18.56 \mu\text{M}$  for citreorosein), probably due to formation of an intramolecular hydrogen bond with the 5-carbonyl group, which hampers binding to UGT1A1. Besides, hydration between the additional hydroxyl groups and the water molecules present in the enzyme might also prevent their interaction with the residues in the binding pocket that would be another cause of the decreased activity, which requires further investigation.

Additionally, 8-Glycosylation of emodin markedly enhanced its inhibitory potency ( $K_i = 3.425 \mu\text{M}$  for emodin-8-O-glu), probably due to the presence of multiple hydroxyl groups on the glucose moiety, providing more sites for binding to UGT1A1. However, rhein ( $K_i = 127.3 \mu\text{M}$ ) and physcion ( $K_i = 94.75 \mu\text{M}$ ) showed extremely weak affinity for UGT1A1, for which two explanations are possible: First, compared with emodin, the 6-hydroxyl groups of rhein and physcion were methylated or absent, and rhein has an additional carboxyl group at C-3 that may affect its interaction with UGT1A1. Second, because the structures of rhein and physcion are similar to that of emodin, whereas their activity and mode of inhibition differ markedly, the former two compounds may bind to other sites of UGT1A1.

Compounds other than those mentioned above were emodin-type dianthrone derivatives (Fig. 1), which can be synthesized from two molecules of emodin via enzyme-catalyzed reduction and intermolecular oxidative coupling reactions<sup>42</sup>. Both trans- and cis-emodin dianthrone exhibited strong inhibitory effects on UGT1A1 ( $K_i = 1.083$  and  $0.863 \mu\text{M}$ , respectively). The two  $\pi$  systems and multiple hydroxyl groups of these two compounds may increase their affinity for UGT1A1 by facilitating hydrophobic interactions and hydrogen bonding.

Because of their large volume and rigidity, the spatial orientation of the tested compounds, which is dependent mainly on the configurations of C10 and C10', influences their binding to UGT1A1. Unfortunately, the trans- and cis-emodin dianthrone tested in this study were racemic mixtures; thus, the relative contributions of the individual pure optical isomers to their inhibitory activities against UGT1A1 are unclear.

Polygonumolides C2–C4 are C10/C10' diastereomers of emodin dianthrone-8-O- $\beta$ -D-glucopyranoside (Fig. 1). The presence of a glucose unit further increases the molecular volume, and the resulting intramolecular hydrogen bonding with the aglycone may stabilize the molecular conformation and thereby enhance their binding stereo-selectivity with UGT1A1, resulting in markedly different levels of inhibition of UGT1A1 ( $K_i = 4.219 \mu\text{M}$  for C2,  $12.89 \mu\text{M}$  for C3, and  $77.42 \mu\text{M}$  for C4).

**Analysis of the interactions between *P. multiflorum* compounds and UGT1A1.** To investigate the mechanism underlying the UGT1A1 inhibitory activities of the *P. multiflorum* compounds, molecular modeling studies were performed (Supplementary Table S1).

Nine active sites of UGT1A1 were identified using the From Receptor Cavities module of Discovery Studio 2.5. The coordinates and radii of the active sites are shown in Supplementary Table S2. All compounds docked into active sites C and F (Fig. 2), depending on their mode of inhibition (Table 1). Emodin, cis-emodin dianthrone, trans-emodin dianthrone, and emodin-8-O-glc showed competitive inhibition, which is consistent with both the docking of the bilirubin substrate into active site F and the *in vitro* inhibition data. The other compounds exhibited non-competitive, mixed-competitive, and un-competitive inhibition and docked primarily into active site C.

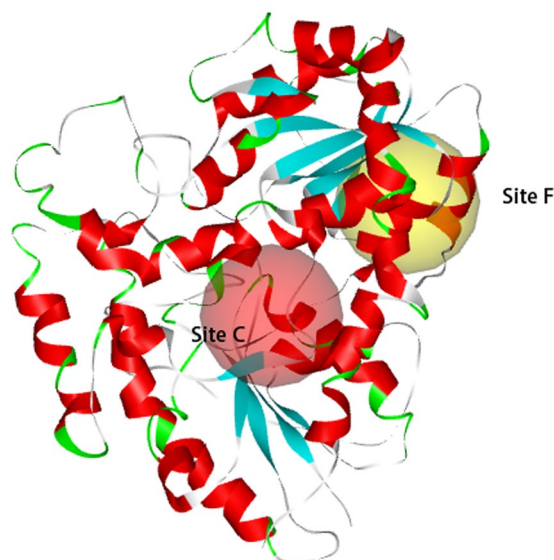


**Figure 2.** The active site C and F in UGT1A1.

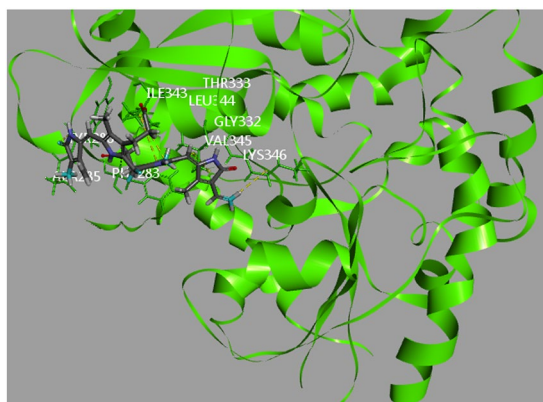


**Figure 3.** Computational docking of bilirubin into the active sites of UGT1A1.

The molecular modeling results revealed that the compounds exhibit hydrophobic interactions with active site F of UGT1A1. These interactions were similar to those between bilirubin and UGT1A1 (Fig. 3).

Among the emodin-type anthraquinones, the skeletons of cieroesein and emodin-8-O-glc displayed  $\pi$ -alkyl hydrophobic interactions similar to those of emodin with ILE343 and VAL345. Moreover, these two compounds showed a  $\pi$ - $\pi$  T-shaped hydrophobic interaction with PHE283, which served to stabilize the complexes (Fig. 4).

In addition to hydrophobic interactions, the hydroxyl groups at the 1- and 8-positions, as well the carbonyl group at the 9-position, of emodin formed hydrogen bonds with LEU344, THR333, and GLY332, respectively. Compared to emodin, the sugar moiety of emodin-8-O-glc formed three additional hydrogen bonds with LYS346, GLY332, and LEU344, although the hydrogen bonds between the aglycone and amino groups were weak. Cieroesein displayed a similar bonding mode to emodin; however, the extra hydroxyl group at the 4-position was not involved in interactions with amino acid residues.

The CDOCKER interaction energies of emodin, cieroesein, and emodin-8-O-glc were  $-25.99932$ ,  $-29.6367$ , and  $-34.7005$  kcal/mol, respectively. These values are not completely in accordance with the inhibition activity ranks: emodin-8-O-glc > emodin > cieroesein. As the crystal structure of UGT1A1 has not been determined, in the homology model water molecules were removed for the position of water molecules could not be determined. It is possible that the additional hydroxyl group in cieroesein results in increased hydration and a weaker interaction between cieroesein and UGT1A1.

In active site F, due to their larger conjugated system, the dianthrone derivatives of cis-emodin dianthrone and trans-emodin dianthrone showed several  $\pi$ -alkyl and  $\pi$ - $\pi$  T-shaped hydrophobic interactions with PHE283, VAL345, and ILE343. Therefore, the hydrophobic interactions of these compounds were much more than those of the emodin-type anthraquinones.



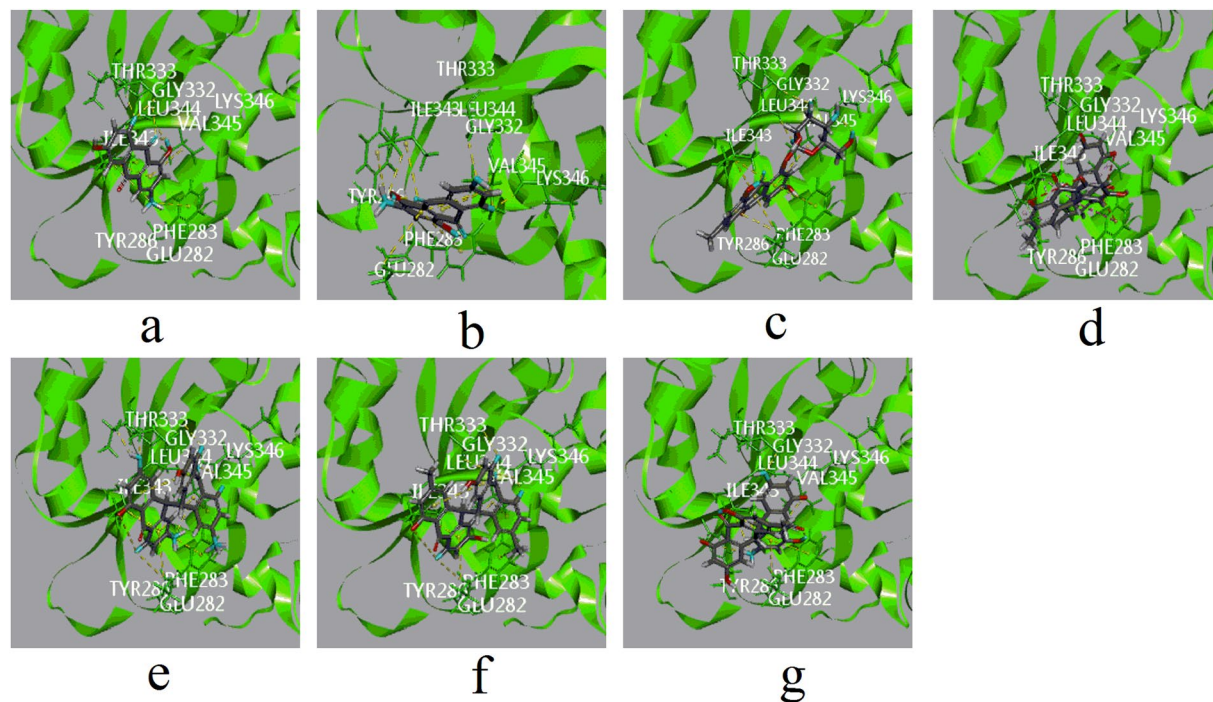


**Figure 4.** Computational docking of ligands in site F. The interaction between ligands and amino acid residues of UGT1A1 (a) emodin with ILE343, VAL345, LEU344, THR333 and GLY332. (b) Citreorosein with ILE343, VAL345, PHE283, LYS346 and GLY332. (c) Emodin-8-O-glc with ILE343, VAL345, PHE283, LYS346, GLY332 and LEU344. (d) Trans-emodin dianthrone (10 $\alpha$ H/10 $\beta$ H) with VAL345, ILE343 and LY332. (e) Trans-emodin dianthrone (10 $\beta$ H/10 $\alpha$ H) with VAL345, ILE343, GLY332, THR333, LYS346 and VAL345 (f) cis-emodin dianthrone (10 $\alpha$ H/10 $\alpha$ H) with VAL345, ILE343, GLY332, LYS346 and VAL345 (g) cis-emodin dianthrone (10 $\beta$ H/10 $\beta$ H) with PHE283, VAL345, ILE343 and GLY332). All involved ligands and side chains by element had been coloured.

As cis-emodin dianthrone and trans-emodin dianthrone are racemic mixtures, different configurations of 10 and 10' affect their space configurations, and the increased molecular volume enhances rigidity, which alters their docking orientations. Trans-emodin dianthrone (10 $\beta$ H/10 $\alpha$ H) and cis-emodin dianthrone (10 $\alpha$ H/10 $\alpha$ H) formed six and five hydrogen bonds with GLY332, THR333, LYS346, and VAL345, respectively, which resulted in low active site C docking energies of  $-42.4254$  and  $-39.8091$  kcal/mol.

In addition to hydrophobic interactions, cis-emodin dianthrone (10 $\beta$ H/10 $\beta$ H) and trans-emodin dianthrone (10 $\alpha$ H/10 $\beta$ H) formed a hydrogen bond with GLY332, which may explain their weaker bonding force with active site F compared with their racemates. The binding energies of cis-emodin dianthrone (10 $\beta$ H/10 $\beta$ H) and trans-emodin dianthrone (10 $\alpha$ H/10 $\beta$ H) were  $-28.2228$  and  $-25.4912$  (kcal/mol), respectively. However, these results were obtained using racemic mixtures of the test compounds.

In active site C (Fig. 5), rhein and physcion showed docking energies of  $-20.6433$  and  $-19.7442$  kcal/mol, respectively, and showed  $\pi$ -alkyl hydrophobic interactions with PRO258. Rhein showed no other interactions with surrounding amino acid residues, which may explain its weaker bonding with UGT1A1. The carboxyl group of rhein may induce hydration, especially in the absence of counterpart basic residues in the binding pocket, which could also be responsible for its relatively weak inhibition of UGT1A1 *in vitro*.

The molecular diameters of polygonumolides C2–4 are 7.5, 8.2, and 8 Å, respectively, which are similar to the size of active site C (7.9 Å). A larger molecular volume leads to enhanced rigidity, which may affect the docking orientation.

No hydrophobic interactions, but six hydrogen bonds with ASN264, MET265, and PRO263, as well as seven intramolecular hydrogen bonds, between polygonumolide C4 and amino acid residues, were detected. The binding energy of polygonumolide C4 ( $-31.1608$  kcal/mol) suggested that its relative lack of hydrophobic interactions might lead to low affinity for UGT1A1.

The binding modes of polygonumolides C2 and C3 ( $\pi$ -alkyl hydrophobic interactions with TRP454 and PRO258) were different from those of polygonumolide C4. Furthermore, polygonumolide C2 formed an additional tight  $\pi$ - $\pi$  stacked hydrophobic interaction with TRP454. Moreover, polygonumolides C2 and C3 were stabilized by hydrogen bonding with ASN264 and PRO258. The CDOCKER interaction energies of polygonumolide C2 and C3 ( $-36.9558$  and  $-37.2953$  kcal/mol, respectively) suggested that these compounds have high affinity for UGT1A1.

Computational docking studies were performed to evaluate the interactions of the tested compounds with UGT1A1. The results suggested that tight hydrophobic interactions are crucial for the affinity between ligands and UGT1A1. The formation of hydrogen bonds via hydroxyl groups enhanced the UGT1A1-binding affinity of the tested compounds.

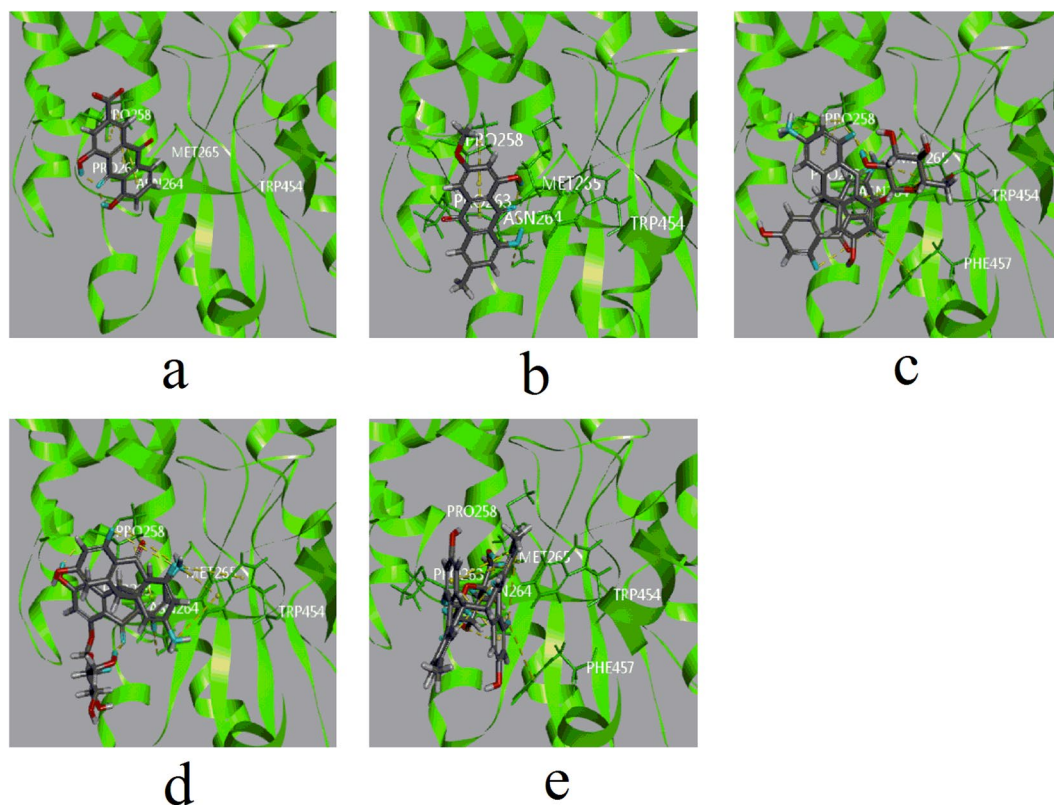


**Figure 5.** Computational docking of ligands in site C. The interaction between ligands and amino acid residues of UGT1A1 (a), rhein with PRO258 ASN264 (b), physcion with PRO258 (c) polygonumnlide C2 with TRP454, PRO258 and ASN264 (d) polygonumnlide C3 with TRP454, PRO258 and ASN264 (e) polygonumnlide C4 with ASN264, MET265 and PRO263). All involved ligands and side chains by element had been coloured.

## Discussion

Quinones are widely distributed in plant species and have multiple pharmacological activities<sup>43</sup>. However, some quinones inhibit UGTs, leading to adverse reactions. For example<sup>44</sup>, OTS167, an antineoplastic agent, is metabolized mainly by UGT1A1 and UGT1A3, and is inhibited by emodin (an inhibitor of UGT1A8 and UGT1A10). At the concentrations required to exert an antitumor effect, celastrol interacts with herbs and drugs<sup>45</sup>. Therefore, determination of the UGT inhibitory effects of quinone compounds is required to enable prediction of drug–drug and herb–drug interactions.

In this study, we evaluated the inhibition of UGT1A1 by a *P. multiflorum* extract and 10 compounds with diverse structures. The *P. multiflorum* extract and several of its anthraquinone and anthrone components inhibited UGT1A1 activity. The *P. multiflorum* extract exhibited a greater inhibitory effect than any of the individual components. The postulated biogenetic relationship among emodin, emodin glucopyranoside, emodin dianthrone (trans-emodin dianthrone and cis-emodin dianthrone), and polygonumnlides C2–C4 may underlie the UGT1A1 inhibitory activity of the *P. multiflorum* extract<sup>42</sup>. As the *P. multiflorum* extract comprises a large number of compounds, the identity and character of the active components should be investigated.

We conducted a mechanistic analysis by the molecular docking method. As the structure of the N-terminal domain of UGT1A1 has not been determined, the crystal structures of four proteins were used as templates. The results were generally consistent with the *in vitro* inhibition data and are in agreement with previous reports that UGT1A1 has at least two binding sites for xenobiotics and endobiotics<sup>46,47</sup>.

The compounds evaluated in this study had an anthraquinone nucleus structure. The molecular modeling indicated that the presence of large conjugated systems (e.g., the dianthronoid derivatives) enhanced hydrophobic interactions with amino acid residues of UGT1A1. However, the large molecular structure of dianthrone and dianthrone glycosides resulted in increased rigidity. The spatial configuration, particularly the 10 or 10' configuration, of a molecule with a diameter equal to or greater than that of the active pocket affects its hydrophobic interactions with amino acid residues.

In conclusion, to our knowledge, this study is the first to evaluate the effects of representative quinone constituents of *P. multiflorum* on UGT1A1 activity *in vitro* and to examine their structure–activity relationships. Notably, cis-emodin dianthrone, trans-emodin dianthrone, and emodin-8-O-glc showed strong inhibition of UGT1A1 and thus warrant particular attention. Moreover, the findings enhance our understanding of the mechanisms underlying *P. multiflorum* toxicity and will facilitate further studies of UGT1A1-mediated drug–drug interactions in patients taking *P. multiflorum*.

## Materials and Methods

**Reagents and materials.** Bilirubin (99.3%), Trizma base, and alamethicin were obtained from J&K Scientific (Beijing, China). Uridine diphosphoglucuronic acid (UDPGA), D-saccharic acid 1,4-lactone, and MgCl<sub>2</sub> were purchased from Sigma-Aldrich (Beijing, China). Pooled male Sprague–Dawley RLM (452501) were obtained from BD Gentest (Shanghai, China). Emodin (99.3%), physcion (99.2%), and rhein (99.8%) were purchased from the National Institute for Food and Drug Control (Beijing, China). Emodin-8-O-glc (98.0%), citreosein (98.0%), trans-emodin dianthrone (98.0%), and cis-emodin dianthrone (98.0%) were purchased from Shanghai Yuanye Bio-Technology Co. (Shanghai, China). Polygonumolides C2, C3, and C4 and the *P. multiflorum* extract were gifts from Dr. Yang (Institute of Materia Medica, Chinese Academy of Medical Sciences & Peking Union Medical College). Polygonumolides C2, C3, and C4 were isolated and characterized by Dr. Yang and colleagues<sup>20</sup>. All other chemicals used in the glucuronidation incubations and the ultra-performance liquid chromatography (UPLC) solvents were of high-performance LC grade and were obtained from Sigma-Aldrich (Beijing, China).

**Preparation of the *P. multiflorum* extract.** Dried roots of *P. multiflorum* (28.0 kg) were extracted three times with 70% ethanol. The extracts were concentrated under reduced pressure at <50 °C, and the resulting concentrated extract (4.0 kg) was used in subsequent experiments.

**Ultra-performance liquid chromatography.** We previously established a complete ultra-performance liquid chromatography (UPLC) method to detect bilirubin glucuronides for the purpose of analyzing the kinetic parameters of UGT1A1<sup>41</sup>. Chromatographic analyses were carried out using an Acquity UPLC system (Waters, Milford, MA, USA) equipped with a binary pump, automatic sampler, photo-diode array detector, system controller, and temperature-controlled oven. Bilirubin and its glucuronides were separated on an Acquity UPLC HSS C18 column (2.1 × 100 mm; 1.8 μm) with a guard column (Acquity UPLC HSS C18 VanGuard pre-column, 2.1 × 5 mm, 1.8 μm). The mobile phase consisted of 0.1% formic acid in water (A) and 100% acetonitrile (B) and was delivered at a flow rate of 0.4 mL/min. The linear gradient elution program was as follows: 0–2.1 min, 40–75% B; 2.1–4.2 min, 75–95% B; 4.2–8.0 min, 95% B; 8.0–8.5 min, 95–40% B. The column temperature was 35 °C. The detection wavelength was 450 nm, and the sample injection volume was 10 μL.

**Assay of UGT1A1 activity.** UGT1A1 activity assays were conducted at 37 °C in a shaking water bath<sup>41</sup>. Incubation mixtures (final volume, 0.2 mL) contained 0.5 mg/mL RLM, 0.1 M Tris-HCl (pH 7.4), 5 mM MgCl<sub>2</sub>, 5 mM D-saccharic acid 1,4-lactone, 3.5 mM UDPGA, and 50 mg/g protein alamethicin. Bilirubin (as a UGT1A1 substrate) and the test samples were dissolved in 100% dimethylsulfoxide (DMSO) immediately before being added to the incubation mixtures. The final DMSO concentration was ≤1%, because preliminary experiments indicated that higher concentrations affect the metabolic activity of liver microsomes. The reaction was initiated by adding UDPGA after a 5-min pre-incubation at 37 °C; it was terminated after 10 min by adding 0.6 mL of ice-cold methanol: acetonitrile (1:2) containing 200 mM ascorbic acid. Proteins were precipitated by centrifugation at 13,000 × g for 30 min at 4 °C prior, and the supernatants were analyzed by UPLC. The assays were done in triplicates respectively.

**Determination of enzyme inhibition kinetics.** Bilirubin glucuronidation was evaluated in the presence of various concentrations of bilirubin and potential inhibitors, as described above. Samples were analyzed in triplicate to determine their inhibition constants (K<sub>i</sub>). For assays with inhibitors, the bilirubin concentration was 0.12 to 1.37 μM. The concentration ranges of the potential inhibitors were as follows: emodin, 0.36–11.6 μM; physcion, 0.15–9.3 μM; rhein, 0.35–11 μM; emodin-8-O-glc, 0.02–3.4 μM; citreosein, 1.45–11.6 μM; trans-emodindianthrone, 0.018–0.29 μM; cis-emodindianthrone, 0.015–0.25 μM; polygonumolide C2, 0.08–1.3 μM; polygonumolide C3, 0.15–2.5 μM; polygonumolide C4, 0.016–0.26 μM; and *P. multiflorum* extract, 1.5–25 μM (because the extract was a mixture, this concentration was based on the highest concentration of emodin).

The inhibition kinetic type and parameters were determined by fitting the reaction velocities of different concentrations of test components (inhibitors) and bilirubin (substrate). Lineweaver–Burk and Dixon fitting equations were employed to determine the inhibition type, and the second plot (drawn using the slope of lines in the Lineweaver–Burk plot versus inhibitor concentrations) was used to calculate the K<sub>i</sub> values. The results were analyzed using GraphPad Prism 5 software (GraphPad Inc., San Diego, CA, USA)<sup>48</sup>. The mean kinetic constants (K<sub>m</sub>, V<sub>max</sub>, and K<sub>i</sub>) ± standard errors are reported. The goodness-of-fit of the inhibition models was estimated using the F statistic, R<sup>2</sup> value, parameter standard error estimates, and 95% confidence intervals<sup>41</sup>. The assays were done in triplicates respectively (Supplementary Fig. S1).

**Computational modeling.** Because the structure of the N-terminal domain of UGT1A1 has not been determined, the properties of the active site of UGT1A1 are unclear. In this study, the BLAST search module of Discovery Studio 2.5 was used to compare amino acid sequence identities and similarities. The following four proteins were selected as templates for homology modeling by the BLAST module: UDP-glucuronosyltransferase 2B7 (PDB: 2O6L), UDP-glucuronosyl/UDP-glucosyltransferase (PDB: 2PQ6), UDP-glucose flavonoid 3-O glycosyltransferase (PDB: 2C1X), and oleandomycin glycosyltransferase (PDB: 2IYA)<sup>49,50</sup>. The similarities were 72%, 43%, 46%, and 54%, respectively, and the identities were 56%, 28%, 27%, and 34%, respectively. The homology models were built using Modeller 9.13. Five candidate models for further optimization were generated by the multi-template modeling method. In this study, all heavy atoms were constrained, the hydrogen atoms were optimized, and the side chains and the loop region were refined based on the energy minimization method, which used the steepest descent method and the conjugate gradient method<sup>51</sup>. Finally, the homology models were



evaluated by generating a Ramachandran plot and Profile-3D analysis<sup>52</sup>. The optimum amount of amino acid residues was 96.37%, and the verify score was 156.27. The verify score suggested that the model structure had good three-dimensional chemical parameters and spatial structure. The CDocker interaction energies were used to evaluate the molecular protein–ligand interactions<sup>53</sup>.

## References

- Xu, M. L. *et al.* A new stilbene glucoside from the roots of *Polygonum multiflorum* Thunb. *Archives of Pharmacol Research* **29**, 946–51 (2006).
- Yu, X. A. *et al.* Influence of different processing times on the quality of *Polygoni Multiflora Radix* by metabolomics based on ultra high performance liquid chromatography with quadrupole time-of-flight mass spectrometry. *J. Sep. Sci.* **40**, 1928–1941 (2017).
- Liang, L. *et al.* Bencao literature investigation of *Polygonum multiflorum* (Heshouwu). *Zhongguo Zhong Yao Za Zhi* **41**, 4456–4461 (2016).
- Zhang, Y. L. *et al.* Effective Components of three kinds of shen-supplementing Chinese medicine on self-renewal and neuron-like differentiation of NSCs in AD mouse embryos: an experimental research. *Zhongguo Zhong Xi Yi Jie He Za Zhi* **34**, 1245–9 (2014).
- Yang, Y. M. *et al.* Suppressive effect *in vitro* of resveratrol on ADP induced human platelet aggregation and its active mechanism. *Yao Xue Bao* **43**, 356–60 (2008).
- He, Q. *et al.* Antiplatelet aggregation bioactivity of *Polygoni Multiflora Radix* with chemical fingerprints and spectrum-effect correlation analysis. *Zhongguo Zhong Yao Za Zhi* **42**, 1679–1684 (2017).
- Muccilli, V. *et al.* Root protein profiles of two citrus rootstocks grown under iron sufficiency/deficiency conditions. *Eur J Mass Spectrom (Chichester)* **19**, 305–24 (2013).
- Li, J. K., Jiang, Z. T. & Li, R. Investigation of antioxidant activities and free radical scavenging of flavonoids in leaves of *Polygonum multiflorum* thunb. *China Food Additives* **2**, 69–74 (2012).
- Li, J. B. & Lin, M. Study on the chemical constituents of *Polygonum multiflorum* Thunb. *Chinese Traditional and Herbal Drugs*. **3**, 115–8 (1993).
- Chen, W. S. *et al.* A new fatty ketone of radix *Polygoni multiflora* preparata. *China Journal of Chinese Materia Medica* **25**, 476–77 (2000).
- Chen, W. S., Zhang, W. D. & Qiao, C. Z. Analysis of the constituents of essential oil from radix *Polygoni multiflora* preparata. *Journal of Chinese Medicinal Materials* **23**, 684–5 (2001).
- Yang, J. B. *et al.* Polygonumolides C1–C4; minor dianthrone glycosides from the roots of *Polygonum multiflorum* Thunb. *J Asian Nat Prod Res* **18**, 813–22 (2016).
- He, D. X. *et al.* Simultaneous determination of five anthraquinones in medicinal plants and pharmaceutical preparations by HPLC with fluorescence detection. *J Pharm Biomed Anal* **49**, 1123–7 (2009).
- Niu, J. H. A severe liver damage case induced by Shou Wu Pian through oral administration. *Chinese Journal of New Drugs and Clinical Remedies* **15**, 382–6 (1996).
- Dong, H. H. *et al.* Eighteen cases of liver injury following ingestion of *Polygonum multiflorum*. *Complementary Therapies in Medicine* **22**, 70–4 (2014).
- Huang, W., Zhang, Y. N. & Sun, R. Experimental study on the “dose-time-toxicity” relationship of acute hepatotoxicity induced by different components from *Polygonum multiflorum* in mice. *Chinese Journal of Pharmacovigilance* **8**, 193–7 (2011).
- Wu, X. Q. *et al.* Toxicity of raw and processed roots of *Polygonum multiflorum*. *Fitoterapia*. **83**, 469–75 (2012).
- Hu, X. Q. *et al.* Experimental study on the toxicology of prepared Radix *Polygoni Multiflora* to the rats’ liver. *Journal of Shaanxi College of Traditional Chinese Medicine* **29**, 40–2 (2006).
- Jung, K. A. *et al.* Drug-Induced liver injury: twenty five cases of acute hepatitis following ingestion of *Polygonum multiflorum* Thunb. *Gut Liver* **5**, 493–9 (2011).
- Dong, H. *et al.* Eighteen cases of liver injury following ingestion of *Polygonum multiflorum*. *Complement. Ther Med* **22**, 70–4 (2014).
- Zhu, Y. *et al.* Causes, features, and outcomes of drug-induced liver injury in 69 children from China. *Gut Liver* **9**, 525–33 (2015).
- Dong, X. *et al.* Aloe-emodin Induces Apoptosis in Human Liver HL-7702 Cells through fas death pathway and the mitochondrial pathway by generating reactive oxygen species. *Phytother Res.* <https://doi.org/10.1002/ptr.5820> (2017).
- Kang, L. *et al.* *Polygoni Multiflora Radix* derived anthraquinones alter bile acid disposition in sandwich-cultured rat hepatocytes. *Toxicol In Vitro*, <https://doi.org/10.1016/j.tiv.2017.01.022> (2017).
- Liu, X. *et al.* Application of ultra high performance liquid chromatography-mass spectrometry to metabolomics study of drug-induced hepatotoxicity. *Se. Pu.* **33**, 683–90 (2015).
- Ma, J. *et al.* Hepatotoxic assessment of *Polygoni Multiflora Radix* extract and toxicokinetic study of stilbene glucoside and anthraquinones in rats. *J Ethnopharmacol* **162**, 61–8 (2015).
- Li, C. L. *et al.* Determination of emodin in L-02 cells and cell culture media with liquid chromatography-mass spectrometry: application to a cellular toxicokinetic study. *J Pharm Biomed Anal.* **71**, 71–8 (2012).
- Nadir, A., Reddy, D. & Van Thiel, D. H. Cascara sagrada-induced intrahepatic cholestasis causing portal hypertension: case report and review of herbal hepatotoxicity. *Am J Gastroenterol* **95**, 3634–7 (2000).
- Soyuncu, S., Cete, Y. & Nokay, A. E. Portal vein thrombosis related to *Cassia angustifolia*. *Clin Toxicol (Phila)* **46**, 774–7 (2008).
- Dong, X. *et al.* Emodin: A Review of its Pharmacology, Toxicity and Pharmacokinetics. *Phytother Res* **30**, 1207–18 (2016).
- Wang, Y. Y. *et al.* Insights into the molecular mechanisms of *Polygonum multiflorum* Thunb-induced liver injury: a computational systems toxicology approach. *Acta Pharmacol Sin* **38**, 719–32 (2017).
- Xia, Y. L. *et al.* Identification and characterization of human UDP-glucuronosyltransferases responsible for the glucuronidation of fraxetin. *Drug Metab Pharmacokinet* **29**, 135–40 (2014).
- Yu, L. *et al.* Hepatic glucuronidation of isoneochamaejasmin A from the traditional Chinese medicine *Stellera chamaejasme* L. Root. *Drug Metab Dispos* **42**, 735–43 (2014).
- Zhu, L. L. *et al.* Diethylstilbestrol can effectively accelerate estradiol-17-Oglucuronidation, while potently inhibiting estradiol-3-Oglucuronidation. *Toxicol Appl Pharmacol* **283**, 109–16 (2015).
- Seppen, J. *et al.* Discrimination between Crigler-Najjar type I and II by expression of mutant bilirubin uridine diphosphate-glucuronosyltransferase. *J Clin Invest* **94**, 2385–91 (1994).
- Mustafa, M. G., Cowger, M. L. & King, T. E. Effects of bilirubin on mitochondrial reactions. *J Biol Chem* **244**, 6403–14 (1969).
- Cowger, M. L. Mechanism of bilirubin toxicity on tissue culture cells - factors that affect toxicity, reversibility by albumin, and comparison with other respiratory poisons and surfactants. *Biochem Med* **5**, 1–16 (1971).
- Shapiro, S. M. Bilirubin toxicity in the developing nervous system. *Pediatr Neurol* **29**, 410–21 (2003).
- Sticova, E. & Jirsa, M. New insights in bilirubin metabolism and their clinical implications. *World J Gastroenterol* **19**, 6398–07 (2013).
- Wang, Q. *et al.* The research of the hepatotoxicity of *Polygonum multiflorum* on the basis of the inhibition of the UGT1A1 enzyme *in vivo* and *in vitro*. *Zhongguo Yao Xue Za Zhi* **51**, 1929–33 (2016).
- Wang, Q. *et al.* Hepatotoxicity of emodin based on UGT1A1 enzyme-mediated bilirubin in liver microsomes. *Zhongguo Zhong Yao Za Zhi* **41**, 4424–7 (2016).
- Wang, Q. *et al.* Estimating the differences of UGT1A1 activity in recombinant UGT1A1 enzyme, human liver microsomes and rat liver microsomes incubation systems *in vitro*. *Journal of biological & pharmaceutical bulletin* **38**, 1910–7 (2015).



42. Yang, J. B. *et al.*  $\alpha$ -Glucosidase inhibitors extracted from the roots of *Polygonum multiflorum* Thunb. *Fitoterapia* **117**, 65–70 (2016).
43. Tingting, T., Daryl, G. & Michael, L. G. A Structural Determinant of Chemical Reactivity and Potential Health Effects of Quinones from Natural Products. *Chem Res Toxicol* **19**(24), 1527–39 (2011).
44. Jacqueline, R. *et al.* Glucuronidation of OTS167 in Humans Is Catalyzed by UDPGlucuronosyltransferases UGT1A1, UGT1A3, UGT1A8, and UGT1A10. *Drug metabolism and disposition* **43**, 928–935 (2015).
45. Zhang, Y. S. *et al.* Strong Inhibition of Celastrol Towards UDP-Glucuronosyl Transferase (UGT) 1A6 and 2B7 Indicating Potential Risk of UGT-based herb-drug interaction. *Molecules* **17**, 6832–9 (2012).
46. Ghosh, S. S. *et al.* Homodimerization of human bilirubin-uridine-diphosphoglucuronate glucuronosyltransferase-1 (UGT1A1) and its functional implications. *J Biol Chem* **276**, 42108–15 (2001).
47. Rios, G. R. & Tephly, T. R. Inhibition and active sites of UDP-glucuronosyltransferases 2B7 and 1 A1. *Drug Metab Dispos* **30**, 1364–7 (2002).
48. Copeland, R. A. *Enzymes: a practical introduction to structure, mechanism, and data analysis*, second edition. New York: Wiley, 266–304 (2002).
49. Song, J. H. *et al.* Inhibition of UDP-Glucuronosyltransferases (UGTs) Activity by constituents of *Schisandra chinensis*. *Phytother Res* **29**, 1658–64 (2015).
50. Li, L. *et al.* Wedelolactone metabolism in rats through regioselective glucuronidation catalyzed by uridine diphosphate-glucuronosyltransferases 1As (UGT1As). *Phytomedicine* **23**, 340–9 (2016).
51. Qiao, L. S. *et al.* Prediction of ETA oligopeptides antagonists from *Glycine max* based on in silico proteolysis. *China J Chin Mater Med* **42**, 746–51 (2017).
52. Zhang, Q. Q. *et al.* Homology Modeling, Molecular Docking, and 3D-QSAR of Indirubin Analogues as CDK1 Inhibitors. *Acta Phys Chim Sin* **30**, 371–81 (2014).
53. Li, Y. *et al.* Discovery of potential ATP-sensitive potassium channel openers with potential hypotensive activity from Chinese herbs based on molecular simulation. *China J Chin Mater Med* **41**, 264–71 (2016).

## Acknowledgements

This work was supported by the National Natural Science Foundation of China (no. 81503347), the National Institutes for Food and Drug Control and Beijing University of Chinese Medicine. The language editing service was provided by Elsevier.

## Author Contributions

Qi Wang conceived and designed the experiments. Qi Wang performed all the experiments and analysed the data. Yadan Wang, Yong Li, Binyu Wen, Zhong Dai, Shuangcheng Ma and Yujie Zhang contributed to manuscript review and approval of the article.

## Additional Information

**Supplementary information** accompanies this paper at <https://doi.org/10.1038/s41598-017-18231-y>.

**Competing Interests:** The authors declare that they have no competing interests.

**Publisher's note:** Springer Nature remains neutral with regard to jurisdictional claims in published maps and institutional affiliations.



**Open Access** This article is licensed under a Creative Commons Attribution 4.0 International License, which permits use, sharing, adaptation, distribution and reproduction in any medium or format, as long as you give appropriate credit to the original author(s) and the source, provide a link to the Creative Commons license, and indicate if changes were made. The images or other third party material in this article are included in the article's Creative Commons license, unless indicated otherwise in a credit line to the material. If material is not included in the article's Creative Commons license and your intended use is not permitted by statutory regulation or exceeds the permitted use, you will need to obtain permission directly from the copyright holder. To view a copy of this license, visit <http://creativecommons.org/licenses/by/4.0/>.

© The Author(s) 2017